Inverse Kinematics and Partial Mass Balancing of a Five-Bar SCARA Robot

Guanglei Wu and Huiping Shen

Abstract This work presents a five-bar SCARA robot with fewer limbs, of which the horizontal position of the robot end-effector is determined by the five-bar mechanism, while the vertical translation and rotation can be independently controlled by means of timing belt transmission embedded in the chamber of the links. The first issue is to solve the inverse kinematic problem of the robot, particularly, the passive rotations of the driven pulleys due to the changed positions of the five-bar links even if the driving pulleys are locked. The second issue is to design mass balancing to reduce the shaking forces of the robot under high-speed motion, without significantly increased overall mass and complex structure. Numerical study verifies the design concept of the proposed five-bar SCARA robot.

1 Introduction

Parallel SCARA robots are well adapted to the pick-and-place operations for fast material handling in various industrial sectors [5]. In general, such robots are composed of three or four kinematic linkages to connect the base and mobile platform [3, 6]. To reduce the structural complexity of linkages, some two-limb parallel SCARA robots are also presented [2], whereas, their actuation structures still include multiple links. Aiming to deploy fewer links to build the manipulator structure, this work presents a parallel SCARA

G. Wu
State Key Laboratory of High-performance Precision Manufacturing, School of Mechanical Engineering, Dalian University of Technology, Dalian 116024, China
e-mail: gwu@dlut.edu.cn

H. Shen
Research Center for Advanced Mechanisms Theory, Changzhou University, Changzhou 213164, China

robot based on the planar five-bar linkage as depicted in Fig. 1, while, the vertical translation and rotation of end-effector can be controlled independently by means of timing belt and pulley transmission embedded in the chamber of the links. As the driven pulley can generate rotations when the rigid links change their positions, the first issue of this work is to handle the kinematics.

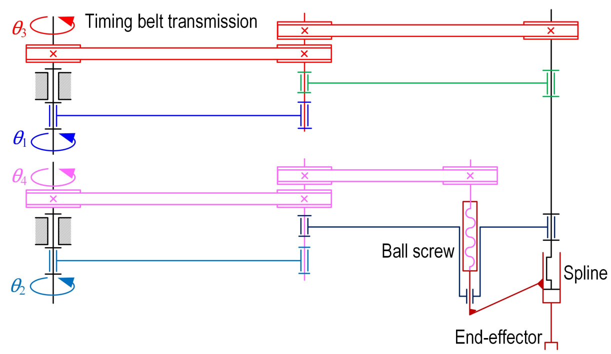

Fig. 1 Kinematic diagram of the five-bar SCARA robot.

Parallel SCARA robots commonly work with high-speed motion, causing large shaking forces exerted to the mounting frame despite the low inertia of structural links, which induces vibration and noise. To improve the dynamic characteristics of such robots, dynamic balancing is essential for their better use [1]. Common approaches to design balanced manipulator include adding counter mass, counter rotating inertia (i.e., mainly adding pairs of gears), and making the manipulator have completely or approximately symmetrical structures, in which a common problem to be encountered lies in the tradeoff between mass/inertial addition (or structural complexity) and space [4].

In light of the two previous issues, this work presents two aspects, namely, kinematic modeling and inertia balancing of the proposed five-bar SCARA robot. Regarding the kinematics, the inverse geometry problem concerning timing belt and pulley transmission system is the focus. On the other hand, to reduce the shaking force, partial balancing is implemented to the five-bar mechanism, which can effectively reduce the inertial forces without significantly increased structural complexity, overall mass and space.

2 Manipulator Under Study

As seen from the kinematic skeleton diagram shown in Fig. 1, the end-effector position projected in the horizontal plane is determined by the five-bar mechanism, while, the vertical translation and rotation of the end-effector can be independently generated via the timing belt and pulley transmissions, namely, two decoupled motions apart from the horizontal movements. Moreover, the combination of the screw pair and the spline results in an equivalent cylindrical pair, to realize the end-effector motion. This design allows an unlimited end-effector rotation. Figure 2 presents a CAD model of the SCARA robot, of which the two driving links are actuated by motors ① and ② by timing belt with a speed ratio. The timing belts and pulleys to generate the decoupled vertical translation and rotation of the end-effector are embedded in the chambers of the links, which are driven by the motors ③ and ④. Most of the components are made up of aluminium alloy for lightweight design and high structural stiffness, and the components as counter masses can be made up of steel with more additional massed installed on it to ensure a compact structure.

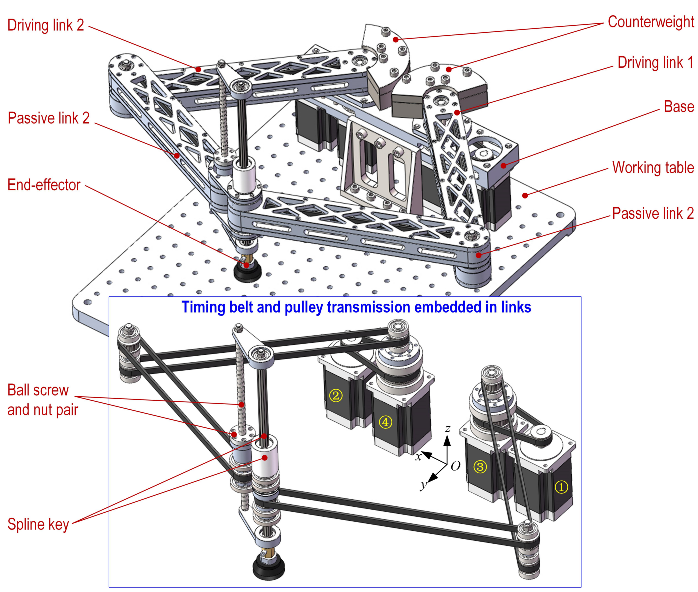

Fig. 2 A rendered CAD model of the five-bar SCARA robot.

3 Kinematics and Jacobian Matrix of the Robot

Since the decoupled motion of the end-effector can be independently controlled, the kinematic and dynamic problems of the overall robot can be readily solved based on the five-bar mechanism. Accordingly, the parameterized structure of the five bar mechanism is shown in Fig. 3, where $\overline{AB} = \overline{CD} = l_1$, $\overline{PB} = \overline{PD} = l_2$, and the origin of the coordinate system is placed on the working table.

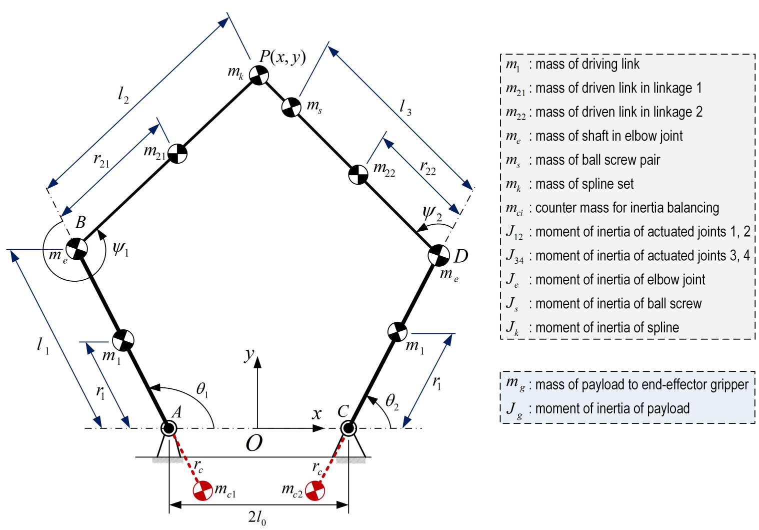

Fig. 3 Parameterizations of the five-bar linkage.

Let the end-effector pose be denoted by $\boldsymbol{\chi} = \begin{bmatrix} x \ y \ z \ \phi \end{bmatrix}^T$, and prior to kinematic and dynamic modeling, the neutral posture of the robot is defined by setting the actuated joint angles as $\theta_1 = \theta_2 = 90°$ and $\theta_3 = \theta_4 = 0°$, subsequently, the coordinates x and y can be solved from the forward kinematic geometry, namely,

$$\begin{bmatrix} x \\ y \end{bmatrix} = \frac{1}{2} l_1 \begin{bmatrix} \cos\theta_1 + \cos\theta_2 \\ \sin\theta_1 + \sin\theta_2 \end{bmatrix} \pm \sqrt{\frac{l_2^2}{l_e^2} - \frac{1}{4}} \begin{bmatrix} l_1 \sin\theta_1 - l_1 \sin\theta_2 \\ 2l_0 - l_1 \cos\theta_1 + l_1 \cos\theta_2 \end{bmatrix} \tag{1}$$

with

$$l_e = \sqrt{4l_0^2 + 2l_1^2[1 - \cos(\theta_1 - \theta_2)] - 4l_0 l_1 (\cos\theta_1 + \cos\theta_2)} \tag{2}$$

It is noteworthy that the sign $\pm$ in Eq. (1) corresponds to two assembly modes of the five-bar mechanism, and here, the mode $+$ is selected, thus, the end-effector pose in neutral configuration is defined by $\boldsymbol{\chi}_0 = \begin{bmatrix} 0 \ l_1 + \sqrt{l_2^2 - l_0^2} \ z_0 \ 0 \end{bmatrix}^T$. Moreover, the intermediate (elbow) joint angles are calculated as

$$\psi_{i0} = (2 - i)2\pi + (-1)^i \sin^{-1} \frac{l_0}{l_2}, \ i = 1, 2 \tag{3}$$

Regarding the inverse kinematic geometry, the joint angles of the five-bar mechanism are solved as

$$\theta_i = 2\tan^{-1}\frac{2yl_1 \pm \sqrt{4l_1^2[(x-(-1)^i l_0)^2+y^2]-[(x-(-1)^i l_0)^2+l_1^2-l_2^2+y^2]^2}}{(l_1+x-(-1)^i l_0)^2-l_2^2+y^2} \tag{4}$$

where the sign $\pm$ in each equation corresponds to the working modes of each linkage, and the $+-$ mode as displayed in Fig. 2 is selected, which can admit a relatively large singularity-free workspace.

Since the pulleys embedded in the joints will produce passive rotations due to the changed positions of links in the five-bar mechanism even if the driving pulleys are locked, the passively changed joint angles corresponding to the vertical translation and rotation of the end-effector can be calculated by means of the varying angles θ_i and ψ_i. With respect to the neutral end-effector posture, the solutions to independent actuated joint angles that are associated with the vertical translation and rotation of the end-effector in any arbitrary configuration $\boldsymbol{\chi} = \begin{bmatrix} x \ y \ z \ \phi \end{bmatrix}^T$ are found as

$$\theta_3 = \phi + \frac{2l_1}{r_{t1}}\sin(\frac{\theta_1}{2}-\frac{\pi}{4}) + \frac{2l_2}{r_{t2}}\sin\frac{\psi_{10}-\psi_1}{2} \tag{5a}$$

$$\theta_4 = 2\pi\frac{z-z_0}{p} + \frac{2l_1}{r_{t1}}\sin(\frac{\pi}{4}-\frac{\theta_2}{2}) + \frac{2l_3}{r_{t2}}\sin\frac{\psi_2-\psi_{20}}{2} \tag{5b}$$

with

$$\psi_i = \pi - (-1)^i\cos^{-1}\frac{l_1^2+l_2^2-(x-(-1)^i l_0)^2-y^2}{2l_1 l_2} \tag{6}$$

where r_{ti} represents the radius of pitch circle of the driven pulley in the driving and passive links, and p depicts the pitch of the ball screw.

Equations (4)-(5b) consist of the inverse kinematic geometry of the five-bar SCARA robot, of which the differentiations with respect to time leads to the forward **A** and inverse **B** Jacobian matrices below

$$\begin{bmatrix} a_{11} & a_{12} & 0 & 0 \\ a_{21} & a_{22} & 0 & 0 \\ a_{31} & a_{32} & 0 & 1 \\ a_{41} & a_{42} & a_{43} & 0 \end{bmatrix} \begin{bmatrix} \dot{x} \\ \dot{y} \\ \dot{z} \\ \dot{\phi} \end{bmatrix} = \begin{bmatrix} b_{11} & 0 & 0 & 0 \\ 0 & b_{22} & 0 & 0 \\ b_{31} & 0 & 1 & 0 \\ 0 & b_{42} & 0 & 1 \end{bmatrix} \begin{bmatrix} \dot{\theta}_1 \\ \dot{\theta}_2 \\ \dot{\theta}_3 \\ \dot{\theta}_4 \end{bmatrix} \quad \Rightarrow \quad A\dot{\boldsymbol{\chi}} = B\dot{\boldsymbol{\theta}} \tag{7}$$

with

$$a_{i1} = x - (-1)^i l_0 - l_1 \cos\theta_i,\ a_{i2} = y - l_1 \sin\theta_i \tag{8a}$$

$$a_{31} = \frac{\sqrt{2}(l_0 - x)\sin(\psi_{20} + \psi_2)}{l_1 r_{t2}\sqrt{1 - \cos(2\psi_2)}},\ a_{32} = -\frac{\sqrt{2}y\sin(\psi_{20} + \psi_2)}{l_1 r_{t2}\sqrt{1 - \cos(2\psi_2)}} \tag{8b}$$

$$a_{41} = \frac{\sqrt{2}(l_0 - x)\sin(\psi_{20} + \psi_2)}{l_1 r_{t2}\sqrt{1 - \cos(2\psi_2)}},\ a_{42} = -\frac{\sqrt{2}y\sin(\psi_{20} + \psi_2)}{l_1 r_{t2}\sqrt{1 - \cos(2\psi_2)}},\ a_{43} = \frac{2\pi}{p} \tag{8c}$$

$$b_{ii} = yl_1\cos\theta_i + (-1)^i l_0 l_1 \sin\theta_i - xl_1\sin\theta_i \tag{8d}$$

$$b_{31} = -\frac{l_1}{r_{t1}}\cos\left(\frac{\theta_1}{2} - \frac{\pi}{4}\right),\ b_{42} = \frac{l_1}{r_{t1}}\cos\left(\frac{\theta_2}{2} - \frac{\pi}{4}\right) \tag{8e}$$

To this end, the kinematic Jacobian matrix can be calculated as $\mathbf{J} = \mathbf{A}^{-1}\mathbf{B}$ as long as matrix $\mathbf{A}$ is nonsingular.

4 Mass Balancing of the Five-bar Mechanism

Aiming to reduce the shaking forces of the robot (here, we focus on the five-bar mechanism) exerted to the fixed frame, a counter mass m_c with counter link as depicted in Fig. 2 can be added to each driving link to balance the inertial forces. To ease the dynamic modeling procedure of the SCARA robot, the method of mass substitution is firstly adopted to make the lumped mass move to the link ends. In accordance with Fig. 3, the mass m_1 can be decomposed to joints $A\,(C)$ and $B\,(D)$, namely,

$$m_{a/c} = \frac{l_1 - r_1}{l_1}m_1,\ {}^1m_{b/d} = \frac{r_1}{l_1}m_1 \tag{9}$$

By the same token, all the masses can be decomposed to the five revolute joints of five-bar linkage, i.e.,

$$m_b = \frac{r_1}{l_1}m_1 + \frac{l_2 - r_{21}}{l_2}m_{21} \tag{10a}$$

$$m_d = \frac{r_1}{l_1}m_1 + \frac{l_2 - r_{22}}{l_2}m_{22} + \frac{l_2 - l_3}{l_2}m_s \tag{10b}$$

$$m_p = m_k + m_g + \frac{r_{21}}{l_2}m_{21} + \frac{r_{22}}{l_2}m_{22} + \frac{l_3}{l_2}m_s \tag{10c}$$

After implementation of mass substitution, the shaking forces exerted to the fixed frame are expressed as

$$\begin{bmatrix} f_x \\ f_y \end{bmatrix} = -m_b l_1 \begin{bmatrix} -\ddot{\theta}_1\sin\theta_1 - \dot{\theta}_1^2\cos\theta_1 \\ \ddot{\theta}_1\cos\theta_1 - \dot{\theta}_1^2\sin\theta_1 \end{bmatrix} - m_d l_1 \begin{bmatrix} -\ddot{\theta}_2\sin\theta_2 - \dot{\theta}_2^2\cos\theta_2 \\ \ddot{\theta}_2\cos\theta_2 - \dot{\theta}_2^2\sin\theta_2 \end{bmatrix} - m_p \begin{bmatrix} \ddot{x} \\ \ddot{y} \end{bmatrix} \tag{11}$$

Recalling Eq. (1), $\ddot{x}$ and $\ddot{y}$ will be calculated by differentiation w.r.t. time in a complex form. Alternatively, Eq. (1) can be rewritten in form of series expansion, by ignoring the high-order terms due to that they have trivial influence to the computation results:

$$\begin{bmatrix} x \\ y \end{bmatrix} \approx \frac{1}{2} l_1 \begin{bmatrix} \cos\theta_1 + \cos\theta_2 \\ \sin\theta_1 + \sin\theta_2 \end{bmatrix} - \frac{1}{2} \left[1 - \frac{1}{2} \left(\frac{l_2}{2l_e} \right)^2 \right] \begin{bmatrix} l_1 \sin\theta_1 - l_1 \sin\theta_2 \\ 2l_0 - l_1 \cos\theta_1 + l_1 \cos\theta_2 \end{bmatrix} \tag{12}$$

Differentiating Eq. (12) w.r.t. time twice leads to the acceleration equation

$$\begin{aligned} \begin{bmatrix} \ddot{x} \\ \ddot{y} \end{bmatrix} &= \frac{1}{2} \ddot{\theta}_1 l_1 \begin{bmatrix} -\sin\theta_1 - \cos\theta_1 \\ \cos\theta_1 - \sin\theta_1 \end{bmatrix} - \frac{1}{2} \dot{\theta}_1^2 l_1 \begin{bmatrix} \cos\theta_1 - \sin\theta_1 \\ \sin\theta_1 + \cos\theta_1 \end{bmatrix} \\ &\quad + \frac{1}{2} \ddot{\theta}_2 l_1 \begin{bmatrix} -\sin\theta_2 + \cos\theta_2 \\ \cos\theta_2 + \sin\theta_2 \end{bmatrix} - \frac{1}{2} \dot{\theta}_2^2 l_1 \begin{bmatrix} \cos\theta_2 + \sin\theta_2 \\ \sin\theta_2 - \cos\theta_2 \end{bmatrix} + \varDelta \\ &= \frac{1}{\sqrt{2}} \ddot{\theta}_1 l_1 \begin{bmatrix} -\sin(\theta_1 + \frac{\pi}{4}) \\ \cos(\theta_1 + \frac{\pi}{4}) \end{bmatrix} - \frac{1}{\sqrt{2}} \dot{\theta}_1^2 l_1 \begin{bmatrix} \cos(\theta_1 + \frac{\pi}{4}) \\ \sin(\theta_1 + \frac{\pi}{4}) \end{bmatrix} \\ &\quad + \frac{1}{\sqrt{2}} \ddot{\theta}_2 l_1 \begin{bmatrix} -\sin(\theta_2 - \frac{\pi}{4}) \\ \cos(\theta_2 - \frac{\pi}{4}) \end{bmatrix} - \frac{1}{\sqrt{2}} \dot{\theta}_2^2 l_1 \begin{bmatrix} \cos(\theta_2 - \frac{\pi}{4}) \\ \sin(\theta_2 - \frac{\pi}{4}) \end{bmatrix} + \varDelta \end{aligned} \tag{13}$$

where $\varDelta$ represents all the complex terms, ignored in the mass balancing. Accordingly, the shaking forces of Eq. (11) can be reduced by means of the design of mass balancing as graphically presented in Fig. 4, i.e., $m_{ci} r_c = m_{li} r_{li}$.

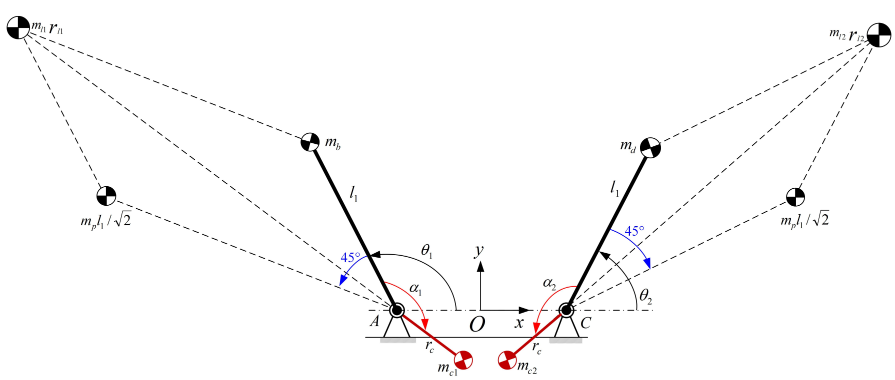

Fig. 4 Graphical presentation of mass-radius and mass balancing of the driving links.

5 Numerical Simulation and Results Discussion

With the CAD model shown in Fig. 2, the structural parameters (unit: m) and mass properties (kg, $\cdot 10^{-3}\text{kgm}^2$) are measured as

$$l_0 = 0.100,\ l_1 = l_2 = 0.460,\ l_3 = 0.385,\ r_1 = 0.212,\ r_{21} = 0.236,\ r_{22} = 0.232$$
$$m_1 = 2.516,\ m_{21} = 2.315,\ m_{22} = 2.444,\ m_e = 0.479,\ m_k = 1.530,\ m_s = 1.059,\ m_g = 1$$
$$J_{12} = 1.292,\ J_{34} = 0.042,\ J_e = 0.073,\ J_s = 0.218,\ J_k = 0.118,\ J_g = 0.223$$

and $m_p l_1/\sqrt{2} \approx 1.8 m_b l_1$, $m_p l_1/\sqrt{2} \approx 1.6 m_d l_1$, which makes $\alpha_1 = 150°$ and $\alpha_2 = 152°$. To ease the mass balancing, the counter link r_c is set opposite to l_1, as the CoM of the counter mass can be readily determined in the manufacturing, thus, the two counter masses are designed as $m_{c1} = 8.323$ and $m_{c2} = 8.915$. Dynamic simulation is carried out along a picking trajectory in Fig. 5(a), and the corresponding varying joint angles are shown in Fig. 5(b).

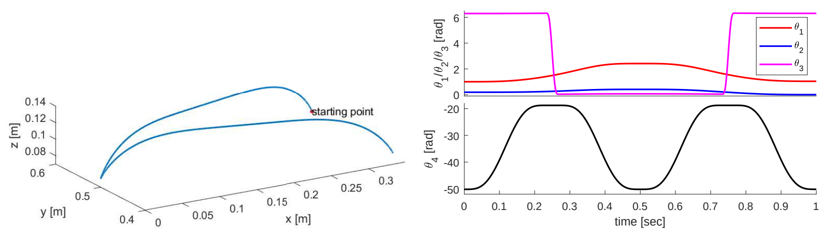

(a) (b)

Fig. 5 (a) test trajectory (rotation $\phi : 0 \rightarrow 2\pi \rightarrow 0$) and (b) joint angle profiles.

The associated simulation results are depicted in Fig. 6, from which it can be seen that after mass balancing of the driving links, the shaking forces can be significantly decreased, particularly, for the peak values of shaking forces with a 50% reduction, although the driving torques slightly increase. By contrast, the shaking moments do not have significant reduction. In this view, a possible way is to adopt set of gears to balance the moments.

6 Conclusions

This work presents a five-bar SCARA robot with a simple structure and unlimited end-effector rotation. The vertical translation and rotation of the robot end-effector can be independently controlled by means of timing blet transmission embedded in the chamber of the links, for which the inverse kinematics is solved considering the passive rotations of the driven pulleys due

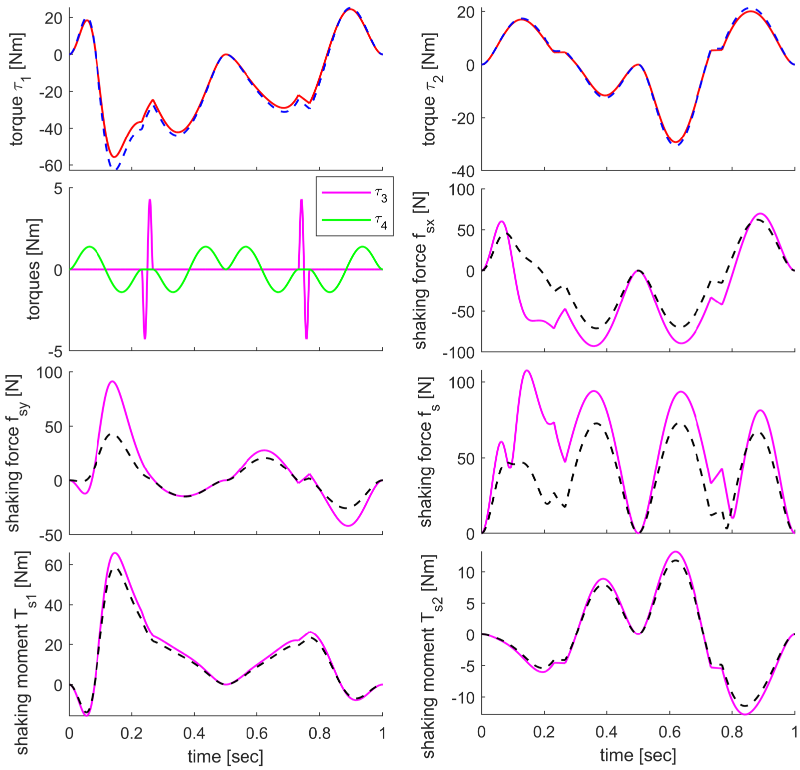

Fig. 6 Dynamic simulation results of the five-bar SCARA robot (solid lines: unbalanced; dashed lines: balanced).

to the changed positions of the five-bar links. A simply design of partial inertia balancing is carried out to reduce the shaking forces, without significantly increased driving torques, which is verified from the simulation results.

Acknowledgements The reported work was supported by National Natural Science Foundation of China (Grant Nos.52575268 and 52375007) and the Fundamental Research Funds for the Central Universities (No. DUTZD25104).

References

1. Acevedo, M., Reyes, J.M.: Dynamic balancing conditions of planar parallel manipulators. In: S. Bai, M. Ceccarelli (eds.) Recent Advances in Mechanism Design for Robotics, pp. 55–64. Springer International Publishing, Cham (2015)
2. Belzile, B., Eskandary, P.K., Angeles, J.: Workspace determination and feedback control of a pick-and-place parallel robot: Analysis and experiments. IEEE Robot. Autom. Lett. **5**(1), 40–47 (2020). DOI 10.1109/LRA.2019.2945468

3. Pierrot, F., Reynaud, C., Fournier, A.: DELTA: a simple and efficient parallel robot. Robotica **8**(2), 105–109 (1990)
4. Vyas, Y.J., van der Wijk, V., Cocuzza, S.: A review of mechanical design approaches for balanced robotic manipulation. Robotics **14**(11) (2025)
5. Wu, G.: Parallel PnP Robots: Dynamic Control and Motion Planning. Springer Nature (2025)
6. Wu, G., Shen, H.: Parallel PnP Robots: Parametric Modeling, Performance Evaluation and Design Optimization. Springer Nature (2021)